Corrosion resistance and passivation behavior of 3004 AlMnMg and 4044AlSi aluminum alloys in acid-chloride electrolytes

To cite this article: Roland T Loto and Moses M Solomon 2021 *Mater. Res. Express* **8** 096529

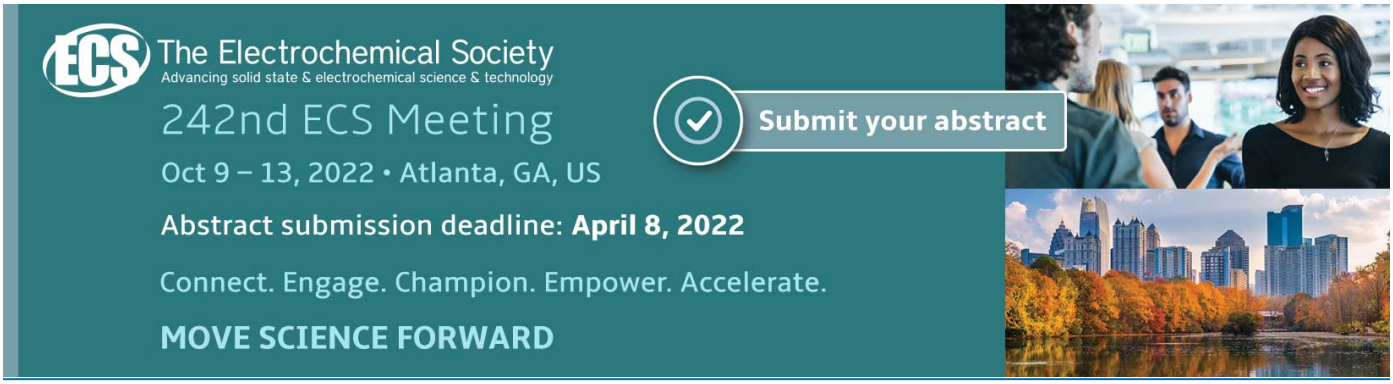

Materials Research Express

PAPER

Corrosion resistance and passivation behavior of 3004 AlMnMg and 4044AlSi aluminum alloys in acid-chloride electrolytes

Roland T Loto[1] **and Moses M Solomon**[2]

[1] Department of Mechanical Engineering, Covenant University, Ota, Ogun State, Nigeria
[2] Department of Chemistry, Covenant University, Ota, Ogun State, Nigeria

E-mail: tolu.loto@gmail.com

OPEN ACCESS

RECEIVED
29 August 2021

REVISED
13 September 2021

ACCEPTED FOR PUBLICATION
20 September 2021

PUBLISHED
30 September 2021

Keywords: corrosion, passivation, pitting, aluminium

Abstract

Corrosion resistance of 3004 and 4044 aluminium alloys (3004Al and 4044Al) in neutral chloride (0.5%–4.5% concentration), sulphate (0.00625M-0.1 M concentration), and chloride-sulphate (0.00625 M H_2SO_4/0.5%–4.5% chloride concentration) solutions was studied with potentiodynamic polarization, open circuit potential, cyclic polarization, and optical microscopy. Results show 4044Al exhibited higher resistance to general corrosion while 3004Al was more resistant to localized corrosion. Corrosion of 4044Al decreases with increase in chloride concentration while 3004 Al increases. Corrosion rate values for 3004Al and 4044Al in sulphate solution were generally similar between 0.061–0.395 mm y^{-1} and 0.168–0.213 mm y^{-1}, respectively. In chloride-sulphate solution, corrosion rate of 3004Al increased from 0.130 mm y^{-1} to 1.563 mm y^{-1} at peak chloride concentration whereas the corrosion rate of 4044Al is near constant. The passive film on 4044Al is found to weaken significantly with increase in chloride concentration. Passivation values varied from 0.39 V at 0.5% chloride concentration to 0.01 V at 4.5% concentration while the potential at which stable pitting occurred increased. The passivation range values for 3004Al are relatively stable with respect to chloride concentration. Results from cyclic polarization experiments show the deterioration rate of both alloys in NaCl solution is subject to chloride concentration. The results show the alloys corrode at all NaCl concentrations (0.5%–4.5%) with the lowest pitting corrosion risk in 0.5% and 1.5%NaCl solutions. The highest pitting corrosion risk of the alloys occurred in 3.5% NaCl solution. Significant localized morphological deterioration is visible throughout the entirety of 4044Al relative to the adjacent Al alloy matrix compared to total surface deterioration on 3004Al.

1. Introduction

Aluminium which constitutes about 8% of all elements within the Earth's crust is an exceptional metallic alloy whose industrial importance ranks second to ferrous alloys as a result of its strength to density fraction, density to weight fraction, conductivity, low temperature stability, reflectivity, non-toxicity, toughness, specific strength, weldability, corrosion resistance, formability, impact resistance and recyclability [1, 2]. The aluminium industry bequeaths about $174 billion to the U.S. economy and yields $70 billion a year in direct economic turnout [3]. Aluminium alloys are broadly utilized in the production of components for industrial, automobile, energy generation, chemical processing, marine and aerospace applications [4–7]. Aluminium properties can be modified to meet the distinct requirements of engineering applications through alteration of their alloying elements and manufacturing conditions. In automobiles and aerospace, aluminium is extensively utilized for economic reasons associated with overall cost reduction in fuel consumption, structural mass and integrity, and durability [3, 8]. Corrosion of aluminium substantially decreases its functional strength leading to structural impairment in the form of cracks, pits, fracture and failure. Unalloyed aluminium metal exhibits sufficient resistance to corrosion degradation due to the evolution of an inert protective oxide on its exterior in mild corrosive environments [9]. Howbeit, its structural strength and application is severely limited necessitating the

need for impartation of different alloying elements. The subsistence of alloying elements within their microstructure generally increases its susceptibility to the electrochemical action of corrosive anions [10–14]. The corrosion behaviour of aluminium alloys in aqueous conditions has been the subject of intensive analysis by reason of its importance in the development of current technologies. The exterior of aluminium is amphoteric in nature and its passive oxide tends to degrade in the presence of threshold concentrations of chlorides, sulphates etc resulting in intergrannular, pitting and general surface deterioration [15, 16].

Different theories have been considered to explain the collapse of the inert oxide on aluminium when corrosive anions transit through the oxide film to the substrate metal. Some researchers concluded that corrosive anions react with the inert oxide causing its dissolution by reason of the formation of metallic complexes [17, 18]. According to Solange *et al* [19], localized deterioration of aluminium alloys in chloride environment is closely associated with the intermetallic second phase and composition. This invariably limits the service potential and industrial importance of the alloy. The oxide on aluminium is generally stable at low anionic concentrations compared to values above the threshold level [20–22]. Results of corrosion of aluminium in cola and citrate-based solutions was shown to be a very slow, time-dependent and complex process strongly influenced by the passivation, complexation and adsorption processes [23]. Corrosion of aluminium was studied in HCl, HNO_3, H_2SO_4 and H_3PO_4 solution with the data output indicating corrosion rate increased with increase in solution concentration and temperature [24]**.** Research on the effect of chloride and sulphate anions on the performance of aluminium based galvanic anodes showed pitting potential lowered as with increase in chloride content while the sulphate anions displayed a passivating effect [25]. Oya *et al* studied the effects of sulfate and sulfite ions on the localized deterioration of aluminium alloy in chloride media by potentiodynamic polarization measurements. Pitting potential tends to nobility at higher sulfate and sulfite ion concentrations. It was ascertained that the sulfate behaved as an inhibitor while the sulfite behaved as an accelerator [26]. Wu and Wu observed the significant effect of SO_4^{2-} ions on the corrosion behaviour of AA7075 aluminium alloy in chloride solution due to competitive anion adsorption mechanism [27].

Other factors which influence the corrosion of aluminium alloys include the temperature of the operating environment, amount and variation of alloying elements and appropriate materials selection. Generally, the atmosphere consists of sulphur and oxides of nitrogen resulting in acid rain. This in addition to seawater are corrosive to aluminium [28]. Application of corrosion inhibitors to suppress the corrosion of aluminium alloys has been proven to be cost effective and sustainable. However, the applicability of this method is severely limited by design requirements, nature of application and toxicity of the inhibitor compound [29–33]. Optimal application of aluminium alloys results from appropriate knowledge of the environments responsible for corrosion, the corrosion type, rate of deterioration and most appropriate preventative technique. Localized corrosion of aluminium is nominally ascertained by the properties, dimension, and arrangement of intermetallic components and secondarily by the characteristics of the solid-solution microstructure of the alloy. This necessitates appropriate choice of materials to mitigate the uneconomical toll of corrosion damage. 3004 AlMnMg aluminum alloy is a non-heat treatable alloy consisting majorly of manganese and magnesium. The alloy is broadly applied in automotive, packaging and building industries due to it is high strength, high corrosion resistance and good machinability. 4044 AiSi aluminum alloy is a wrought aluminum-silicon alloy which cannot be heat-treated. The addition of Si to the aluminum microstructure reduces the melting point of the aluminum alloy. This enables its versatile application as a casting alloys and filler material in welding of aluminum components. This research studies and compares the corrosion behaviour and localized corrosion resistance of 3004 AlMnMg and 4044 AiSi aliminum alloys in neutral chloride and sulphate-environment for optimal alloy application.

2. Materials and methods

3004 AlMnMg alloy (3004Al) gotten from the power steering pump of an automobile and 4044 AlSi alloy (4044Al) gotten from the master brake cylinder of an automobile was analysed at Aluminium Rolling Mills, Ota, Ogun State to determine its nominal (wt%) composition (table 1). The alloys prepared with manual hacksaw to give five (5) test pieces with square configuration (1 cm^2). The pieces were afterwards set encased in pre-hardened resin paste with an exposure alloy exterior area of 1 cm^2 after setting of the paste. The mounted 3004Al and 4044Al test pieces were grinded with coarse abrasive papers (60, 120, 320, 600, 800 and 1000 grits) and burnished to 6 μm before washing with H_2O and $(CH_3)_2CO$. Analytical grade NaCl purchased from Titan Biotech, India was concocted in percentage concentrates of 0.5%, 1.5%, 2.5%, 3.5% and 4.5% in 200 ml of condensed H_2O while analytical grade H_2SO_4 from Sigma Aldrich, USA was concocted in molar concentrates of 0.00625 M, 0.0125 M, 0.025, 0.05 M and 0.1 M H_2SO_4 solution respectively.

Potentiodynamic polarization analysis was done at temperature of 30 °C with Digi-Ivy 2311 potentiostat coupled to a computer. Polarization plots were produced at sweep rate of 0.0015 V s^{-1} from potential of −1.5 V

Table 1. Percentage nominal composition of 3004Al and 4044Al.

							3004Al								
Element symbol	Sn	Si	Ti	Zn	Mn	Mg	Pb	Ni	Fe	Cr	Sr	Zr	V	Co	Al
%Wt composition	—	0.3	0.03	0.25	1.1	1.15	—	—	0.7	—	—	—	—	—	96.07
							4044Al								
Element Symbol	Sn	Si	Ti	Zn	Mn	Mg	Pb	Ni	Fe	Cr	Sr	Zr	V	Co	Al
%Wt composition	0.02	7.26	0.03	0.03	0.39	0.46	0.02	0.03	0.42	0.02	0.004	0.008	0.022	0.01	91.25

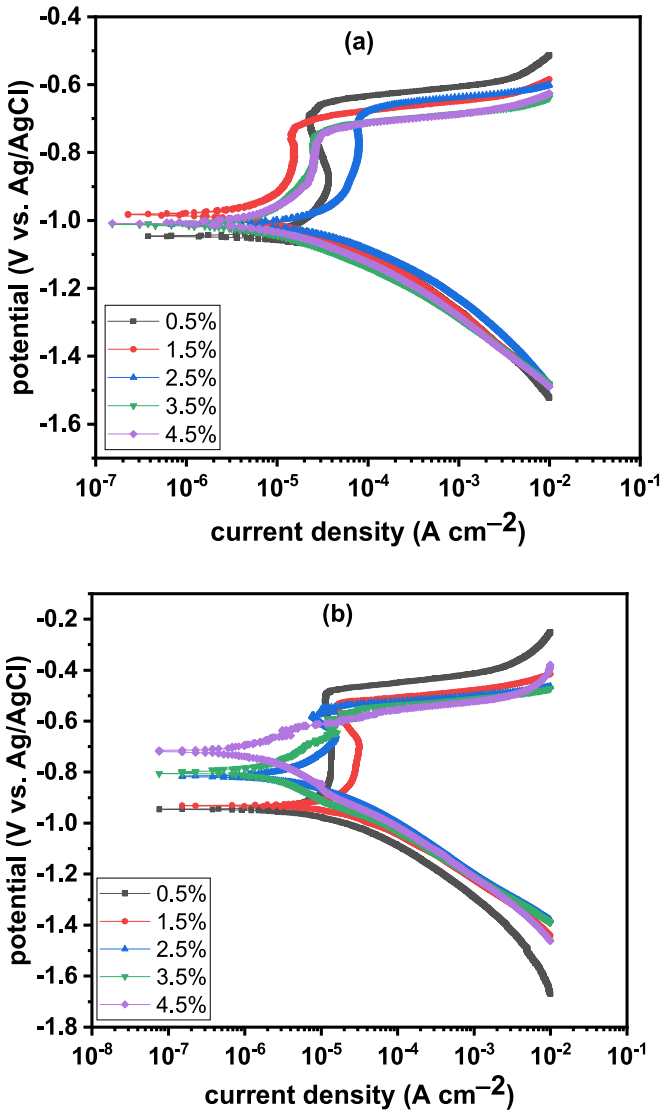

Figure 1. Potentiodynamic polarization plots of (a) 3004Al alloy and (b) 4044 Al alloy in different concentrations of NaCl at 30 °C.

and +1 V. The CPDP experiments were conducted using initial potential of −0.25 V/E_{OCP}, apex/reverse potential of +1 V/E_{OCP}, and final potential of 0 V/E_{OCP} with forward and reverse scan rate of 0.2 m V s^{-1}. Electrochemical parameters (corrosion current density, C_{cd} (A/cm^2) and corrosion potential, C_{pt} (V) values were determined from the plots by Tafel extrapolation. Corrosion rate, C_{Rt} (mm/y) was obtained from the mathematical illustration below (equation (1));

$$C_{Rt} = \frac{0.00327 \times C_{cd} \times E_q}{D} \quad (1)$$

D illustrates density in (g/cm^3); E_q represents the metal alloy equivalent weight (g) while 0.00327 represents the constant for corrosion rate. Open circuit potential measurement (OCP) was performed at 2 V s^{-1} step potential for 10800 s to retrieve information on active/passive transition behavior of the alloy in the electrolytes. Optical illustrations of 3004Al and 4044Al test pieces were studied with Omax trinocular metallurgical microscope.

3. Results and discussion

3.1. Potentiodynamic polarization studies

The potentiodynamic polarization plots in figures 1(a) and (b) illustrates the corrosion behaviour of 3004Al and 4044Al alloy in neutral chloride solutions (0.5%–4.5% NaCl concentration). Figures 2(a) and (b) show the polarization plots of 3004Al and 4044Al alloys from H_2SO_4 solution (0.00625 M to 0.1 M concentration) while figures 3(a) and (b) show the plots of the aluminium alloys from the chloride-sulphate solution (0.00625 M H_2SO_4/0.5%–4.5% NaCl concentrations). Tables 2–4 depicts the polarization data for 3004Al and 4044Al

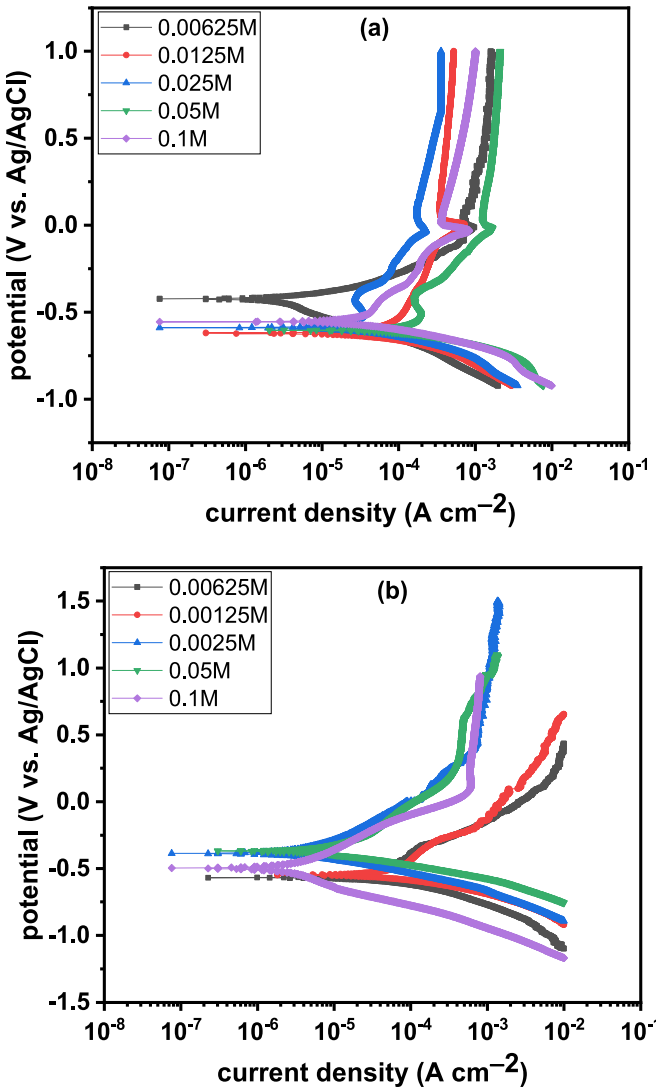

Figure 2. Potentiodynamic polarization plots of (a) 3004Al alloy and (b) 4044 Al alloy in different concentrations of H_2SO_4 solution at 30 °C.

retrieved during potential scanning at pre-set values from the chloride, sulphate and sulphate-chloride solutions, respectively. Variation of the cathodic polarization plots in figures 1(a) and (b) are relatively minimal signifying the cathodic reduction reaction mechanisms (H_2 evolution and O_2 reduction) is under activation control according to equations (2)–(4) below.

$$2H^+ + 2e^- \rightarrow H_2 \quad (2)$$

$$O_2 + 2H_2O + 4e^- \rightarrow 4OH^- \quad (3)$$

$$O_2 + 4H^+ + 4e^- \rightarrow 2H_2O \quad (4)$$

However, the slope configuration shows that the cathodic reaction mechanisms on 4044Al [figure 1(b)] is more significant within the overall corrosion process and strongly influences the corrosion potential of the alloy compared to 3004Al [figure 1(a)]. The anodic portion of the polarization plots for 3004Al shows limited dissolution reactions which arises from partial breakdown of the protective oxide layer on the alloy and formation of soluble complexes before extended passivation behaviour [34, 35]. During anodic polarization, the electrolytic transport of Al^{3+} ion occurs through the ionized alloy surface into the electrolyte at which the corrosion current density increases with Cl^- ion concentration. At higher Cl^- ion concentration, displacement of OH^- ions from the alloy surface causes higher adsorption of Cl^- and net effect increase in corrosion [36]. This is later suppressed by the formation of a thin film of Al_2O_3 during upward scanning on both alloys resulting in the visible passivated region of the plots [37–39]. 4044Al showed stable passivation behaviour at 0.5% and 1.5% NaCl concentration similar to 3004Al at all NaCl concentration. At 2.5% NaCl, instability of the passive region for 4044Al occurred due to weakening of the protective oxide, whereas at 3.5% and 4.5% NaCl concentration significant collapse of the passive region is visible due to dominant anodic dissolution reactions. The presence of

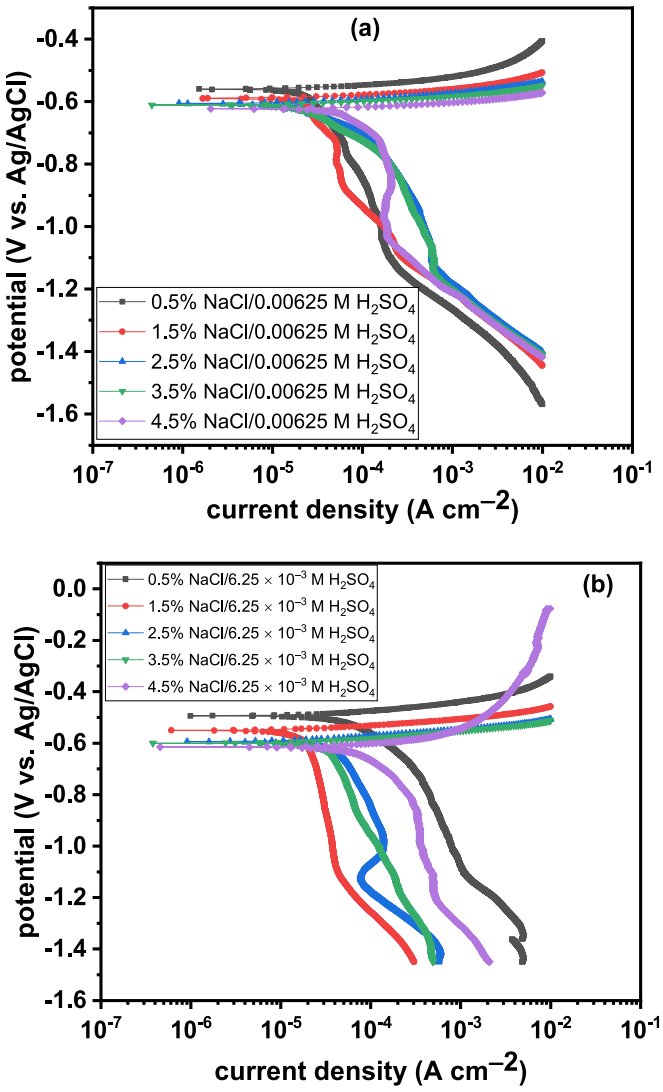

Figure 3. Potentiodynamic polarization plots of (a) 3004Al alloy and (b) 4044 Al alloy in 0.00625 M H_2SO_4 solution in combination with 0.5%–4.5% NaCl solution at 30 °C.

Si probably limited the continuity of the oxide film on 4044Al as a result of the formation of galvanic couples between the aluminium substrate and the precipitates. Hence, the active sites on the alloy increases with increase in chloride concentration as shown in the current transients present on the anodic plots of 4044Al at 3.5% and 4.5% NaCl concentration [40]. The strong affinity of 3004Al for O_2 is responsible for its strong resistance to localized deterioration at all NaCl concentrations and evidently transforms 3004Al to $Al(OH)_3$ (equation (5)). The passivated region on 3004Al extends to the transpassive region where localized dissolution of the protective film in the form of pits occurs.

$$Al + 3OH^- \rightarrow Al(OH)_3 + 3e^- \quad (5)$$

The corrosion rate of 3004Al at 0.5% NaCl concentration is 0.233 mm y^{-1} corresponding to corrosion current density of 1.78 × 10^5 A cm^{-2} and polarization resistance of 1443 Ω. This value is significantly higher that the corresponding value for 4044Al due to greater redox electrochemical processes occurring on 3004Al surface. The non-metallic characteristics of Si within the microstructure of 4044Al contributes to this feature. The electrochemical reaction of chloride on the alloy surface can be summed up in the equations (equations (6)–(13)) below;

$$Al \rightarrow Al^{3+} + 3e^- \quad (6)$$

$$Al^{3+} + H_2O \rightarrow Al(OH)^{2+} + H^+ \quad (7)$$

Table 2. Potentiodynamic polarization parameters for 3004Al and 4044Al alloy corrosion in 0.5% – 4.5% NaCl solution.

			3004Al				
NaCl Conc. (%)	Corrosion Rate (mm/y)	Corrosion Current (A)	Corrosion Current Density (A/cm^2)	Corrosion Potential ($V_{Ag/AgCl}$)	Polarization Resistance, R_p (Ω)	Cathodic Tafel Slope B_c (V/dec)	Anodic Tafel Slope B_a (V/dec)
0.5	0.233	1.78E-05	1.78E-05	−1.046	1443.00	−10.080	2.800
1.5	0.680	6.11E-05	6.11E-05	−0.982	324.00	−10.810	3.473
2.5	0.987	8.87E-05	8.87E-05	−1.121	289.80	−8.562	2.819
3.5	1.048	9.41E-05	9.41E-05	−1.038	259.00	−9.331	4.099
4.5	1.168	1.05E-04	1.05E-04	−1.007	244.80	−9.911	5.037
			4044Al				
0.5	0.078	6.99E-06	6.99E-06	−0.946	3677.00	−9.092	2.633
1.5	0.051	4.55E-06	4.55E-06	−0.931	4657.00	−9.461	2.903
2.5	0.043	3.85E-06	3.85E-06	−0.817	6673.00	−9.594	4.884
3.5	0.025	2.21E-06	2.21E-06	−0.806	11610.00	−6.876	6.405
4.5	0.013	1.18E-06	1.18E-06	−0.719	21790.00	−6.705	2.147

Table 3. Potentiodynamic polarization parameters for 3004Al and 4044Al corrosion in H_2SO_4 solution (0.00625M-0.1 M concentration).

			3004Al				
H_2SO_4 Conc. (M)	**Corrosion Rate (mm/y)**	**Corrosion Current (A)**	**Corrosion Current Density (A/cm^2)**	**Corrosion Potential** ($V_{Ag/AgCl}$)	**Polarization Resistance, R_p (Ω)**	**Cathodic Tafel Slope B_c (V/dec)**	**Anodic Tafel Slope B_a (V/dec)**
0.00625	0.061	4.64E-06	4.64E-06	−0.425	5535.00	−5.947	9.671
0.0125	0.342	3.07E-05	3.07E-05	−0.680	975.60	−8.653	3.456
0.025	0.661	5.93E-05	5.93E-05	−0.589	630.70	−10.540	1.059
0.05	1.042	9.36E-05	9.36E-05	−0.605	188.60	−10.410	1.616
0.1	0.395	3.55E-05	3.55E-05	−0.555	723.70	−11.450	1.061
			4044Al				
0.00625	0.168	1.51E-05	1.51E-05	−0.568	1706.00	−9.777	4.291
0.0125	0.422	3.79E-05	3.79E-05	−0.548	678.00	−0.104	3.187
0.025	0.051	4.59E-06	4.59E-06	−0.387	5604.00	−5.299	4.569
0.05	0.079	7.13E-06	7.13E-06	−0.368	4139.00	−0.106	8.165
0.1	0.213	1.91E-05	1.91E-05	−0.496	316.40	−11.390	3.257

Table 4. Potentiodynamic polarization data for 3004Al and 4044Al in 0.00625 M H_2SO_4 solution +0.5%–4.5% NaCl concentration.

			3004Al				
0.00625 M H_2SO_4 /NaCl Conc. (%)	**Corrosion Rate (mm/y)**	**Corrosion Current (A)**	**Corrosion Current Density (A/cm^2)**	**Corrosion Potential** ($V_{Ag/AgCl}$)	**Polarization Resistance, R_p (Ω)**	**Cathodic Tafel Slope B_c (V/dec)**	**Anodic Tafel Slope B_a (V/dec)**
0.5	0.130	9.90E-06	9.90E-06	−0.491	6125.00	−4.840	11.590
1.5	0.648	5.82E-05	5.82E-05	−0.550	441.20	−1.168	17.260
2.5	0.678	6.09E-05	6.09E-05	−0.594	421.90	−2.357	18.360
3.5	0.822	7.39E-05	7.39E-05	−0.600	347.80	−1.615	20.540
4.5	1.563	1.40E-04	1.40E-04	−0.615	183.00	−4.090	7.080
			4044Al				
0.5	1.090	9.79E-05	9.79E-05	−0.560	262.50	−5.011	11.110
1.5	1.261	1.13E-04	1.13E-04	−0.590	226.80	−3.021	9.853
2.5	1.306	1.17E-04	1.17E-04	−0.606	214.50	−7.833	3.741
3.5	1.372	1.23E-04	1.23E-04	−0.611	208.60	−6.481	0.117
4.5	1.505	1.35E-04	1.35E-04	−0.623	190.00	1.789	15.460

$$Al^{3+} + Cl \rightarrow AlCl^{2+} \quad (8)$$

$$Al(OH)^{2+} + Cl^{-} \rightarrow Al(OH)Cl^{+} \quad (9)$$

$$AlCl^{2+} + 2H_2O \rightarrow Al(OH)_2Cl + 2H^{+} \quad (10)$$

$$Al(OH)Cl^{+} + H_2O \rightarrow Al(OH)_2Cl + H^{+} \quad (11)$$

$$Al(OH)_2Cl + H_2OAl(OH)_3 + H^{+} + Cl^{-} \quad (12)$$

$$2Al(OH)_3(amorphous) \rightarrow \gamma Al_2O_3.H_2O(boehmite) + 2H_2O \quad (13)$$

Increase in Cl^- ion concentration results in increase in corrosion rate of 3004Al culminating at 1.168 mm y^{-1} (4.5% NaCl concentration) while the corrosion rate of 4044Al decreases with increase in NaCl concentration culminating at 0.013 mm y^{-1}. The higher chloride concentration accelerated the weakening of the protective oxide on the alloy on 3004Al beyond the passive region whereby chemically combined O_2 molecules at the metal oxide interface are displaced by Cl^- ions through competitive adsorption and displacement reactions [41]. This results in the formation of weak surface complexes which further exposes the substrate metal to corrosion. The significant variation in the anodic polarization plots on 4044Al compared to 3004Al shows the corrosion reaction mechanism is more anodically controlled i.e. a diffusion controlled corrosion process where NaCl concentration strongly influences the positive shift in corrosion potential values of the alloy.

The corresponding corrosion rate values of 3004Al in H_2SO_4 solution [table 3] are generally lower than the values obtained from the neutral chloride solution. This contrast the values obtained for 4044Al alloy in H_2SO_4 solution, whose values in H_2SO_4 are higher than the values obtained in the chloride media. The reason for this observation is due to the differences in the metallurgical structure of both alloys i.e. the grain orientation, formation of intermetallic precipitates and the resulting electrochemical structure of the passive film. At 0.00625 M H_2SO_4 solution, corrosion rate of 3004Al is 0.061 mm y^{-1}. The corrosion rate value peaked at 0.05 M H_2SO_4 solution (1.042 mm y^{-1}) before declining to 0.395 mm y^{-1} at 0.1 M H_2SO_4 solution. This observation occurred for two reasons. Firstly, the sulphate solution is probably weaker than the neutral chloride solution or as a result of the larger molecular size of sulphates. Secondly, the complexes formed from reaction of SO_4^{2-} ions with the alloy surface are less soluble (equations (14) and (15)) compared to the reaction products from the neutral chloride solution. However, previous research has shown that SO_4^{2-} anions displays passivating effect on some aluminium alloys [25]. Considering the electrochemical observations of 4044Al and the resulting corrosion rates from H_2SO_4 and NaCl solutions, its more probable to establish the fact that microstructural properties of alloys tend to have a dominant effect compared to the elemental constituents of electrolytes considering the corrosion rate values of 4044Al from H_2SO_4 and NaCl solution and comparing it to the corresponding values for 3004Al

$$Al^{3+} + SO_4^{2-} \rightarrow AlSO_4^{2-} \quad (14)$$

$$Al(OH)^{2+} + SO_4^{2-} \rightarrow Al(OH)SO_4^{2-} \quad (15)$$

The short cathodic polarization plots for 3004Al and 4044Al [figures 2(a) and (b)] results from increase in cathodic polarization slope configuration due to increase in H_2 evolution and O_2 reduction reactions. These reactions are more significant on 4044Al, though it influences the corrosion behaviour of both alloys in H_2SO_4 solution. The significant departure of cathodic plots of both alloys from linearity shows the overall reaction kinetics is diffusion controlled. According to Trowsdale *et al* [42] the presence of Si in Al alloy is responsible for the occurrence of breakages, flaws etc on the passive film and formation of galvanic couples as earlier mentioned. This results in microstructural heterogeneities and increases the active sites on the alloy. Hence, the wider variation in cathodic polarization slopes of 4044Al and the resulting corrosion potential [43]. The anodic slope region shows significant anodic dissolution reaction on both alloy surfaces which is also a function of the ohmic resistance and concentration of the acid electrolyte. Though limited or short passivation behaviour occurred at some electrolyte concentrations in [figure 2(a)] due to the formation of a porous oxide film [44], this was completely absent in [figure 2(b)]. The film eventually in [figure 2(a)] due to ionic diffusion at the oxide/electrolyte interface [45].

Observation of the corrosion rate values in table 4 shows the combined electrochemical action of SO_4^{2-} and Cl^- ions on 3004Al and 4044Al surfaces strongly influenced their rate of deterioration. Comparing the corrosion rate of both alloys, it is evident that 3004Al displayed a higher corrosion resistance in 0.00625 M H_2SO_4 from 0.5%–3.5% NaCl concentration. The values initiated at 0.130 mm y^{-1} (0.5% NaCl) and peaked at 0.822 mm y^{-1} (3.5% NaCl). The corresponding values for 4044Al within this range is between 1.090 mm y^{-1} and 1.372 mm y^{-1}. This observation is due to the strength of 3004Al passive film which was able to withstand the ionic transport of the corrosive species [46, 47], secondly the rate of formation of its passive film is probably much faster. Judging from another perspective, the corrosion rate of 3004Al in the chloride-sulphate solution is relatively (slightly) lower than the values obtained in NaCl solution (0.5%–3.5% NaCl). This signifies that the presence of SO_4^{2-} ions within the chloride-sulphate solution has a passivating effect on the microstructural properties of 3004Al due to competitive adsorption mechanism in displacing the adsorbed O_2 molecules. Quite

the contrary was observed for 4044Al in chloride-sulphate and chloride solution. The presence of combined SO_4^{2-} and Cl^- ions had a more deleterious effect on the protective oxide on 4044Al compared to Cl^- ions only. At 4.5% NaCl concentration in table 4, the corrosion rate of 3004Al and 4044Al are comparable signifying the threshold Cl^- ion concentration on 3004Al that severely weakens it passive film. The corrosion potential shift shows cathodic reduction reactions dominated the corrosion process. However, the cathodic plot configuration shows 3004Al corrosion underwent dominant diffusion-controlled processes compared to 4044Al.

3.2. Passivation and pitting corrosion studies

Passivation and pitting corrosion on 3004Al and 4044Al alloy surfaces were evaluated through potentiostatic studies. Table 5 shows the potentiostatic parameter values obtained to study the localized corrosion resistance and susceptibility of the alloys. Al passivates in the presence of corrosive ions due to adsorption of dissolved O_2 atoms within the electrolyte forming a protective oxide barrier. According to Bennour *et al* [48], Ralston *et al* [49] and Serna *et al* [50], the oxide act as kinetic inhibitors which stifles further anodic degradation of the substrate Al alloy. Table 5 shows 4044Al generally passivates at higher potentials (less electronegative potentials) relative to its corrosion potential compared to the corresponding values for 3004Al. Increase in Cl^- ion concentration shifts the potential at which 4044Al passivates. This is probable due to the anodic shift in corrosion potential of 4044Al, signifying dominant oxidation reactions related to its passive film formation and breakdown. The passivation range values for 4044Al confirms this assertion where significant decrease in value, related to the instability and subsequent weakening of the passive film occurred. Judging from the general corrosion rate values in table 2, it is clearly visible that 4044Al exhibits weak resistance to localized corrosion due to weak formation of its protective oxide, but exhibits higher resistance to general corrosion. The presence of Si, the main alloying element for 4044Al alloy improves its strength but results in the formation of intermetallic particles, second phases and precipitates which invariably introduce micro-galvanic cells across the alloys surface. The occurrence of the cells is with respect to their dimensions and distribution microstructure of the alloy. Invariably results in a heterogeneous microstructural exterior protected by discontinuous protective oxide. Cl^- ions reacts with the defects in the passive layer resulting in localized deterioration [51–57]. As a result, the potential at which pitting occurs on 4044Al (table 5) relative to the passivation potential significantly decreases. The passivation range 3004Al were relatively stable after 0.5% NaCl concentration. This shows stability and resilience of its passive film in the face of debilitating action of Cl^- ions with respect to concentration [58–64] shows Mn reduces the potential difference between the Al substrate matrix and intermetallic phases, while Mg is highly soluble within Al microstructure in the solid state and slows down the rate of cathodic reaction. Hence the higher corrosion exhibited by 3004Al to localized corrosion. However, thinning of the protective oxide may occur but observation of the potentials at which passivation and pitting occurred there is evidence to suggest that the passive film on 3004Al remained stable at all Cl^- ion concentrations before breakdown at the transpassive region of the polarization plots leading to stable pitting behaviour.

The influence of NaCl concentration on the pitting corrosion of 3004Al and 4044Al alloys in NaCl solution at normal atmospheric pressure and at 30 °C was further studied using the cyclic polarization technique (CPDP). Figure 4 shows the cyclic potentiodynamic polarization plots for 3004Al alloy in different concentrations of NaCl solution at 30 °C. The obvious effect of concentration on the pitting corrosion of the alloy can be clearly seen. An incomplete positive hysteresis loop is observed in figure 4(a) (0.5% NaCl). That is, the current densities in the reverse scan are higher than the current densities of the forward scan [64, 65]. Normally, a positive hysteresis is indicative of the breakdown of passive film and its inability to self-repair or pits initiation [64]. The fact that the loop did not cross the anodic arm as expected tends to suggest the inability of the oxide passive film to repassivate in 0.5% NaCl solution. The shape of the polarization curve suggests active corrosion process in which mass transport of species played a significant role. As could be seen in the figure, the cathodic branch is inclined at about 45° and is consistent with diffusion-controlled corrosion process [66]. In the studied NaCl concentrations, diffusion is related to the reduction of dissolved oxygen at the cathodic region [65]. From the analysis, the corrosion potential (E_{corr}), corrosion current density (i_{corr}), and the corrosion rate (C_{Rt}) of the alloy in 0.5% NaCl solution is $-0.645V_{Ag/AgCl}$, 3.129 μA cm^{-2}, and 0.034 mm y^{-1}, respectively.

Figures 4(b)–(d) show the CPDP of 3004Al alloy in 1.5%, 2.5%, and 3.5% NaCl solution, respectively. In the figures, relative to figure 4(a), a different corrosion phenomenon is observed. The hysteresis loop is complete and the direction of the reverse scan is reversed. That is, the current densities in the reverse scan are lower than those of forward scan and this defines a negative hysteresis [64, 65]. The completeness of the hysteresis loop may suggest occurrence of localized pitting corrosion and the possibility of repassivation. The negative hysteresis loop is indicative of a possible self-repair of damaged passive film [64, 65]. A comparison of the hysteresis loop in figures 4(b)–(d) reveals that the size increases with an increase in the concentration of NaCl. According to

Table 5. Potentiostatic data for passivation and pitting corrosion resistance of 3004Al and 4044Al corrosion in NaCl solution (0.5%–4.5% NaCl concentration).

			3004Al			
NaCl Conc. (%)	**Corrosion Potential** ($V_{Ag/AgCl}$)	**Passivation Potential** ($V_{Ag/AgCl}$)	**Passivation Current (A)**	**Stable Pitting Potential** ($V_{Ag/AgCl}$)	**Stable Pitting Current (A)**	**Passivation Range** ($V_{Ag/AgCl}$)
0.5	−1.046	−0.99	2.00E-05	−0.65	4.00E-05	0.34
1.5	−0.982	−0.94	1.00E-05	−0.68	1.00E-04	0.26
2.5	−1.121	−0.94	4.00E-05	−0.68	1.10E-04	0.26
3.5	−1.038	−0.96	1.00E-05	−0.72	5.00E-05	0.24
4.5	−1.007	−0.96	1.00E-05	−0.73	5.00E-05	0.23
			4044Al			
0.5	−0.946	−0.88	1.09E-05	−0.49	1.22E-05	0.39
1.5	−0.931	−0.85	2.35E-05	−0.54	1.74E-05	0.31
2.5	−0.817	−0.65	1.53E-05	−0.55	1.07E-05	0.10
3.5	−0.806	−0.64	1.31E-05	−0.57	1.94E-05	0.07
4.5	−0.719	−0.65	3.42E-06	−0.64	3.11E-06	0.01

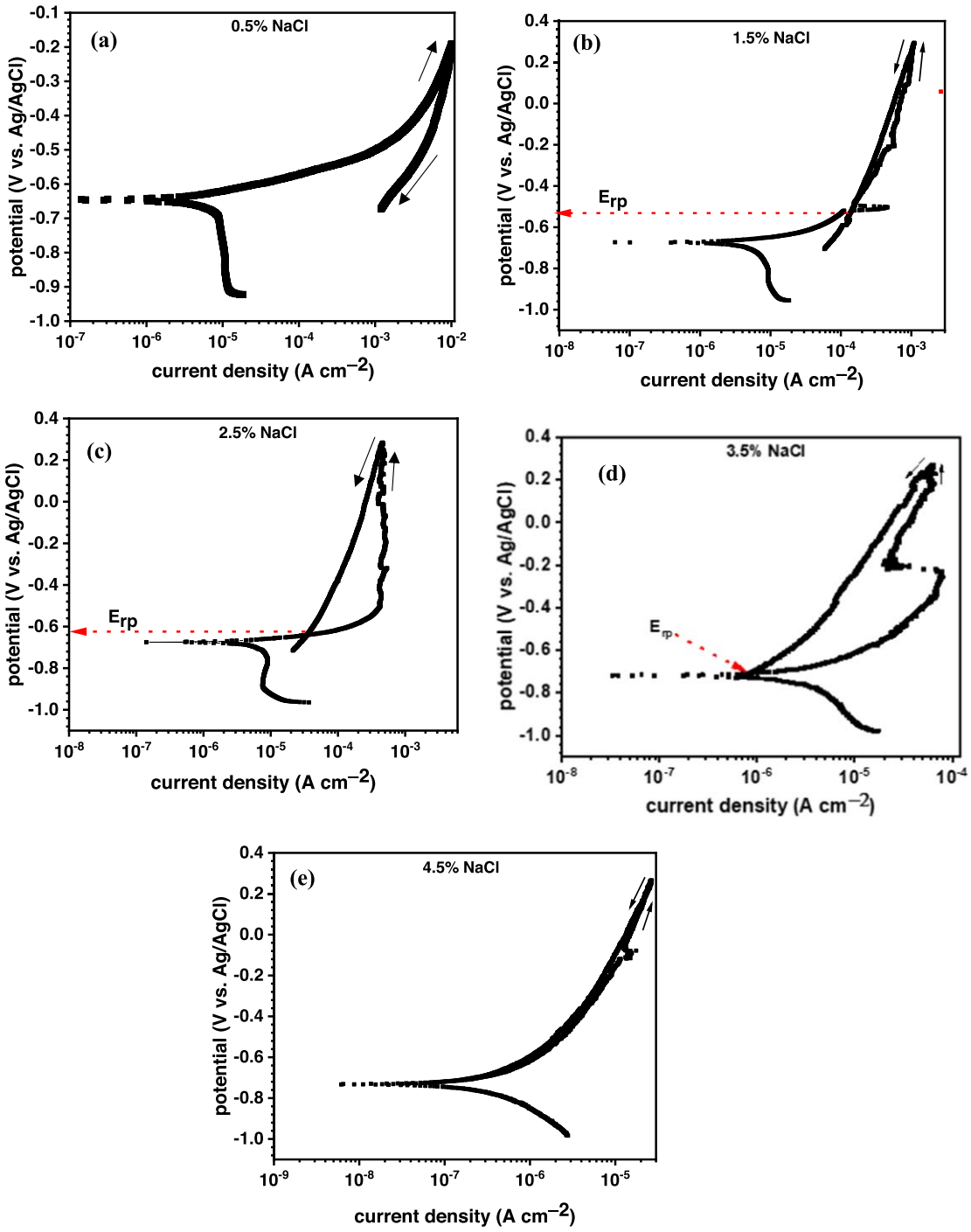

Figure 4. Cyclic potentiodynamic polarization plots for 3004Al alloy in different concentrations of NaCl solution at 30 °C.

Esmailzadeh *et al* [65], the bigger size of hysteresis loop, the greater the disruption of passive film and more difficult to restore.

In figures 4(b)–(d), E_{rp} denotes repassivation potential. This is the potential by which the propagation of pits stopped [64, 65]. The E_{corr} and E_{rp} can be used to evaluate the resistance of a material to localized corrosion [64, 65]. Generally, a nobler E_{rp} value compared to E_{corr} value indicates stoppage of propagation pits [64, 65]. It means that, at the potentials lying between E_{rp} and E_{corr}, a stable passive film is formed and there is no initiation of new pits [64]. Also, crevice corrosion is diminished [65]. Old pits only grow at the potentials before E_{rp}. In the other hands, if the E_{corr} value is nobler than the E_{rp} value, repassivation of pits will not occur and pits propagation continues unabatedly [65]. For the corrosion of 3004Al alloy in 1.5% NaCl solution, the E_{corr}, E_{rp}, i_{corr}, and C_{Rt} values are $-0.667V_{Ag/AgCl,}$ $-0.527V_{Ag/AgCl}$, 3.991 μA cm^{-2}, and 0.044 mm y^{-1}, respectively. Because the E_{rp} value is nobler than the E_{corr} value, we submit that a perfect passivity where there is no pitting and crevice corrosion exist at potentials lying between $-0.527V_{Ag/AgCl}$ (E_{rp}) and $-0.667V_{Ag/AgCl}$ (E_{corr}).

Similarly, the E_{corr}, E_{rp}, i_{corr}, and C_{Rt} values in 2.5% NaCl solution are $-0.675V_{Ag/AgCl}$, $-0.654V_{Ag/AgCl}$, 4.272 μA cm^{-2}, and 0.048 mm y^{-1}, respectively. Although the E_{rp} value is nobler relative to the E_{corr} value, it could be seen that there are very close to each other. It means that the perfect passivity region is narrower compared to that of the 1.5% NaCl system. Consequently, a higher corrosion rate is obtained in 2.5% NaCl solution. In 3.5% NaCl solution, the E_{corr}, E_{rp}, i_{corr}, and C_{Rt} values are $-0.717V_{Ag/AgCl}$, $-0.723V_{Ag/AgCl}$, 5.320 μA cm^{-2}, and 0.058 mm y^{-1}, respectively. In this concentration, the E_{rp} is more negative than the E_{corr} and the highest corrosion rate of 0.058 mm y^{-1} is recorded due to the dissolution of the metal [66, 67].

Figure 4(e) shows the CPDP plot for 3004Al alloy in 4.5% NaCl solution. The graph is devoid of hysteresis loop as the reverse scan coincided with the forward scan. This is interpreted as the absence of localized corrosion [65]. The nature of the graph rather points to an active surface and general corrosion of the alloy in 4.5% NaCl solution [68]. This observation is in agreement with the report of Asaduzzaman *et al* [68]. Asaduzzaman and co-workers studied the effect of concentration on the pitting corrosion of austenitic stainless steel in aqueous chloride solution and reported an active corrosion in 4.5% NaCl solution. The authors had explained that in 4.5% NaCl solution relative to 3.5% NaCl, pit initiation time (induction time) was lesser due to the higher anodic-hold potential in the passive region. The more positive the hold potential in the passive range, the less is the pit initiation time. The E_{corr}, i_{corr}, and C_{Rt} values obtained for this system are $-0.732V_{Ag/AgCl}$, 609.0 μA cm^{-2}, and 6.65 $\times$ 10^{-5} mm y^{-1}, respectively.

The CPDP results obtained for 4044Al corrosion at different concentrations of NaCl solution are presented in figure 5. The CPDP graphs in 0.5% [figure 5(a)] and 1.5% [figure 5(b)] NaCl solutions are defined by an incomplete positive hysteresis loop, hence we ruled out repassivation tendency in 0.5% and 1.5% NaCl solutions and associate the deterioration of 4044Al alloy in these media to active corrosion [66]. From the analysis of the CPDP data, corrosion potential (E_{corr}), corrosion current density (i_{corr}), and the corrosion rate (CR) of the alloy in 0.5% NaCl solution are $-0.669V_{Ag/AgCl}$, 1.546 μA cm^{-2}, and 0.017 mm y^{-1}, respectively. Similarly, the E_{corr}, i_{corr}, and CR of the alloy in 1.5% NaCl solution are $-0.730V_{Ag/AgCl}$, 7.180 μA cm^{-2}, and 0.079 mm y^{-1}, respectively. The E_{corr} value is nobler and the i_{corr} is lesser in 0.5% NaCl solution relative to 1.5% NaCl medium. Consequently, the alloy corroded faster in 1.5% NaCl than in 0.5% NaCl solution. The CPDP graphs in figures 5(c)–(e) exhibit different features from the graphs in figures 5(a) and (b). For instance, there is complete hysteresis loop in figures 5(c)–(e) and anodic nose (active-passive transition) also exist. This indicates the occurrence of pitting corrosion and repassivation of the alloy in the higher concentrations of NaCl solution [69]. CPDP results can be interpreted using parameters such as E_{corr}, pitting potential (E_{pit}), E_{rp}, and the anodic nose [69]. E_{pit} is the potential at which pit develops and/or grows. At this potential, the current density increases rapidly [65, 69]. The difference between E_{pit} and E_{rp} ($E_{pit} - E_{rp}$) is indicative of the extent of resistance to localized corrosion [65, 69]. Additionally, if the anodic nose is nobler than *E*corr, it means that the material is passivating and can easily restore damaged surface oxide films [65, 69]. The difference between anodic nose and *E*corr is usually used to ascertain the persistence of passive film [65, 69]. A high value of anodic nose $-E_{corr}$ infers unstable passive film at *E*corr [69]. The values of the afore-described electrochemical parameters obtained for the corrosion of 4044Al alloy in 2.5%–4.5% NaCl solutions are summarized in table 6. It is observed in figure 5(c) that the reverse scan crosses at the cathodic arm and in table 6, the E_{corr} value for the 2.5% NaCl solution is nobler than E_{rp} and Anodic nose. These observations point to an unstable passive film on the alloy surface. It means that the potential of the corroded areas (E_{rp} and Anodic nose) is more negative than the uncorroded area (E_{corr}), leading to the corroded areas serving as anodic regions and continuing to corrode such that pits propagate to depth. Similar to the behaviour of 3004Al, 3.5% NaCl solution is more aggressive than 4.5% NaCl solution. For instance, the $E_{pit} - E_{rp}$ and the anodic nose $-E_{corr}$ values are higher in 3.5% NaCl solution than in 4.5% NaCl solution (table 6) meaning the alloy oxide film was more stable in 4.5% NaCl solution than in 3.5%, which again is in agreement with the report of Asaduzzaman *et al* [68].

3.3. Open circuit potential measurements

The active-passive transition behaviour of 3004Al and 4044Al in NaCl (0.5% and 4.5% concentration), H_2SO_4 (0.00625 M and 0.1 M concentration) and NaCl-H_2SO_4 (0.00625 M H_2SO_4/0.5% and 4.5% NaCl concentration) solutions was studied for 7200 s. Figure 6(a) shows the open circuit potential (OCP) plots for 3004Al and 4044Al in NaCl solution, figure 6(b) shows the OCP plots of both alloys in H_2SO_4 solution while figure 6(c) shows the OCP plots for the alloys in NaCl-H_2SO_4 solution. The microstructural properties of both aluminium alloys within the electrolytes significantly influences their electrochemical structure of the electric double layer at the electrode/solution interface which invariably influences the extent of polarization of the alloys. The corrosion potential is also influenced by the properties of the electrolyte, corrosion reactions at the alloy surface, rate of dissolution and formation of precipitates. The OCP plot for 4044Al alloy at 0.5% NaCl concentration exhibited the most electropositive transition behaviour while at 4.5% NaCl concentration its plot configuration was the most electronegative [figure 6(a)]. 3004Al and 4044Al generally displayed significant

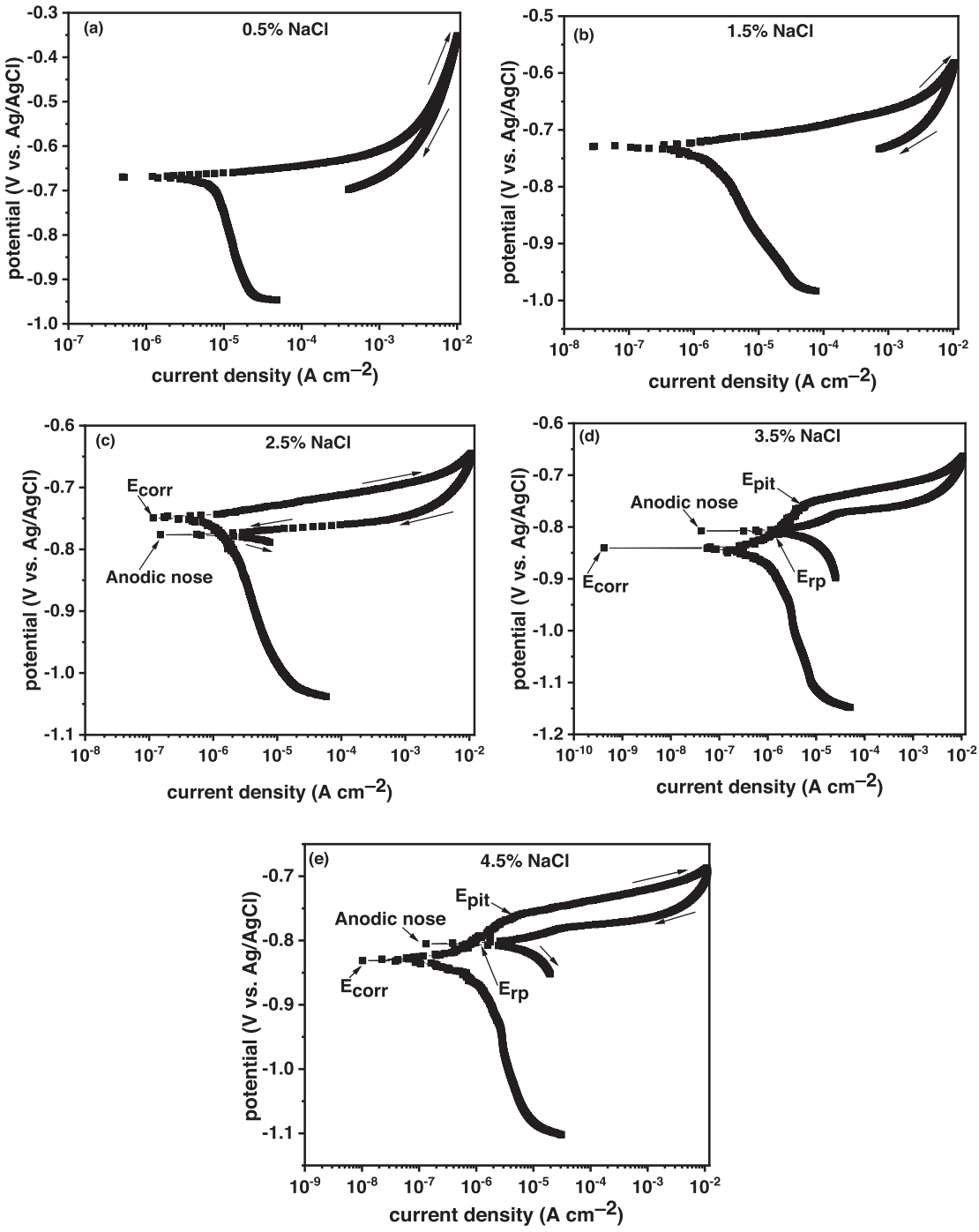

Figure 5. Cyclic potentiodynamic polarization plots for 4044Al alloy in different concentrations of NaCl solution at 30 °C.

passivation behaviour and thermodynamic stability in the chloride solution. The plots initiated at values between $-0.817V_{Ag/AgCl}$ and $-1.113V_{Ag/AgCl}$ and shifted sharply to electropositive values at 200 s ($-0.679V_{Ag/AgCl}$) and 1033 s ($-0.667V_{Ag/AgCl}$) due to the instantaneous formation of the protective oxide on the alloy surface. Despite its higher electropositive values, the OCP plot of 4044Al displayed visible potential transients due to instability of its passive film compared to the plot for 3004Al at 0.5% NaCl. The instantaneous breakdown and reformation of the passive film is responsible for the potential transients. This phenomenon is prevalent in the presence of sites on the alloy microstructure where non-metallic inclusions and discontinuities of the passive film is present. The corresponding plot for 3004Al shows its passive film is thermodynamically stable due to relative homogeneity of its passive film and there is a gradual transition to electropositive potentials.

The corrosion potentials of the OCP plots in figure 6(b) are relatively higher than the values obtained in figure 6(a). Secondly, the plot configuration shows 3004Al exhibited higher corrosion resistance than 4044Al at

Table 6. Electrochemical parameters for 4044Al alloy in NaCl solution from CPDP.

NaCl conc. (%)	$-E_{corr}$ ($V_{Ag/AgCl}$)	$-E_{pit}$ ($V_{Ag/AgCl}$)	$-E_{rp}$ ($V_{Ag/AgCl}$)	$E_{pit}-E_{rp}$ ($V_{Ag/AgCl}$)	−Anodic nose ($V_{Ag/AgCl}$)	Anodic nose $-E_{corr}$ ($V_{Ag/AgCl}$)
2.5	0.749	—	0.774	—	0.777	−0.027
3.5	0.841	0.764	0.804	0.040	0.807	0.034
4.5	0.831	0.768	0.802	0.034	0.805	0.026

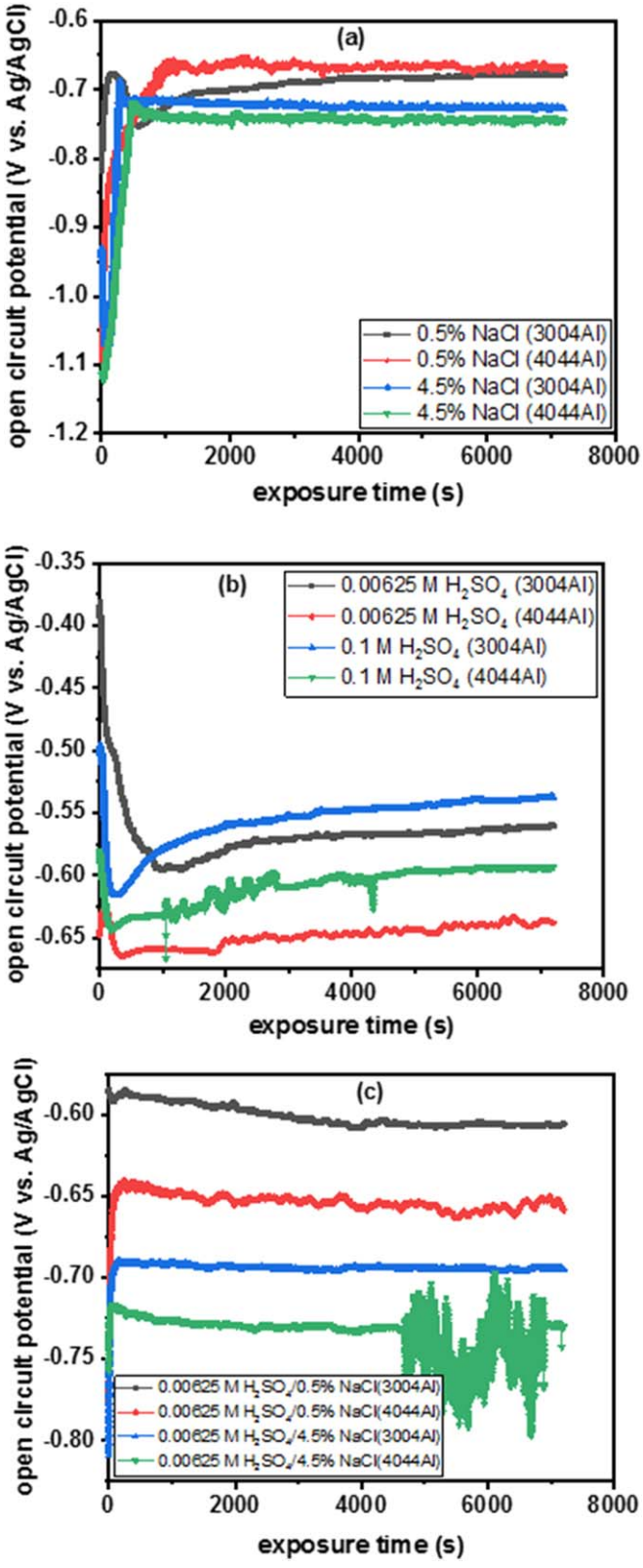

Figure 6. Open circuit potential plots for 3004Al and 4044Al in (a) NaCl solution at 0.5% and 4.5% concentrations, (b) H_2SO_4 solution at 0.00625 M and 0.1 M concentrations, and (c) NaCl−H_2SO_4 solution at 0.5% and 4.5% NaCl concentrations.

0.00625 M and 0.1 M H_2SO_4 solution. This observation is probably due to the passivating effect of SO_4^{2-} ions on 3004Al. Secondly. It is probable the SO_4^{2-} ions were unable to penetrate the passive film with respect to their weak concentration. This observation is further confirmed from the lower corrosion rate values obtained in H_2SO_4 solution compared to NaCl from polarization test. 3004Al OCP plots at 0.00625 M and 0.1 M H_2SO_4 solutions initiated at −0.393 V and −0.503 V (0 s) and sharply declined to $-0.583V_{Ag/AgCl}$ and $-0.616V_{Ag/AgCl}$

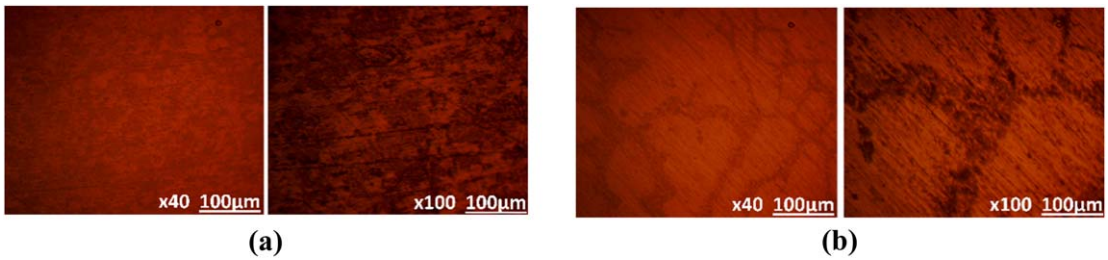

Figure 7. Microscopic images of (a) 3004Al and (b) 4044Al before corrosion test.

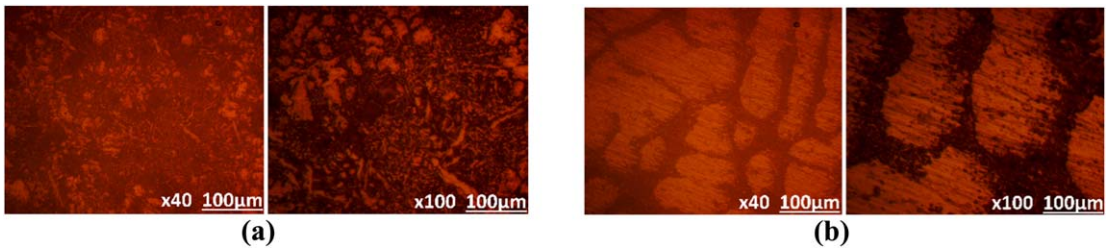

Figure 8. Microscopic images of (a) 3004Al and (b) 4044Al from 0.5% NaCl solution.

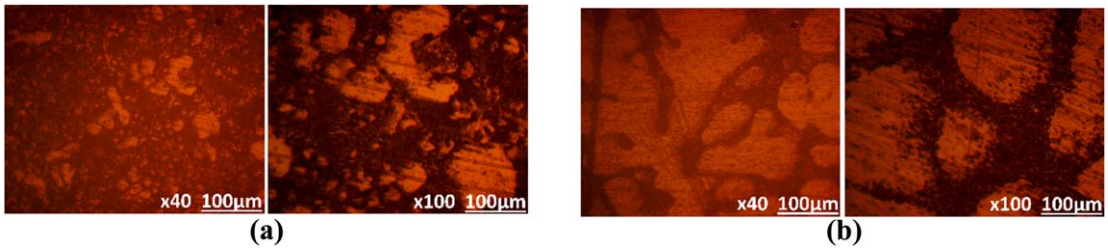

Figure 9. Microscopic images of (a) 3004Al and (b) 4044Al from 4.5% NaCl solution.

at 862.81 s and 240.2 s due to initial breakdown of the passive film and corrosion of the substrate alloy. Beyond this point a gradual increase in corrosion potential value was observed before relative stability due formation of the protective oxide. Comparing theses plots to the plot configuration of 4044Al at 0.00625 M and 0.1 M H_2SO_4 concentration, the lower corrosion potential shows passive film formed on 4044Al Al is much weaker and prone to the deteriorating effect of SO_4^{2-} ions. In the presence of combined sulphate-chloride solution [figure 6(c)], the corrosion resistance and thermodynamic stability of 3004Al in 0.00625 M H_2SO_4 at 0.5% NaCl concentration increased compared to NaCl and H_2SO_4 solution. The competitive adsorption process contributes to the passivating effect of the corrosive ions on the alloy surface. The corrosion potential of the alloy initiated at $-0.586V_{Ag/AgCl}$ (0 s) and culminated at $-0.606V_{Ag/AgCl}$ (7200 s). Relative improvement was observed for 4044Al alloy with the same solution for reasons earlier mentioned. Its plot configuration initiated at $-0.779V_{Ag/AgCl}$ (0 s) and sharply increased to $-0.644V_{Ag/AgCl}$ at 239.20 s due to evolution of its passive film aided by the passivating effect of the electrolyte. However, the plots for 3004Al and 4044Al in 0.00625 M H_2SO_4 at 4.5% NaCl concentration showed marginal increase in corrosion resistance of the alloy compared to their corresponding plots in figure 6(a). The plots culminated at $-0.695V_{Ag/AgCl}$ and $-0.730VA_{g/AgCl}$ at 7200 s compared for their value in figure 6(a) at $-0.728\ V_{Ag/AgCl}$ and $-0.745\ V_{Ag/AgCl}$ (7200 s).

3.3.Optical microscopic studies

Optical microscopic images of 3004Al and 4044Al at specific anionic concentration were obtained and studied at magnification ×40 and ×100. Figures 7(a) and (b) shows the optical images of 3004Al and 4044Al before corrosion. Figures 8(a) to 9(b) shows the optical images of 3004Al and 4044Al from NaCl solution at 0.5% and 4.5% concentration. Figures 10(a) to 11(b) shows the optical images of 3004Al and 4044Al from H_2SO_4 solution at 0.00625 M and 0.1 M concentration, while figures 12(a) to 13(b) shows the optical images of 3004Al and

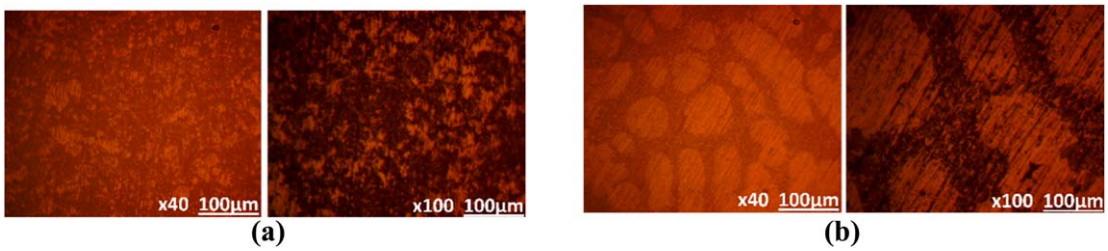

Figure 10. Microscopic images of (a) 3004Al and (b) 4044Al from 0.00625 M 0.1 M H_2SO_4 solution.

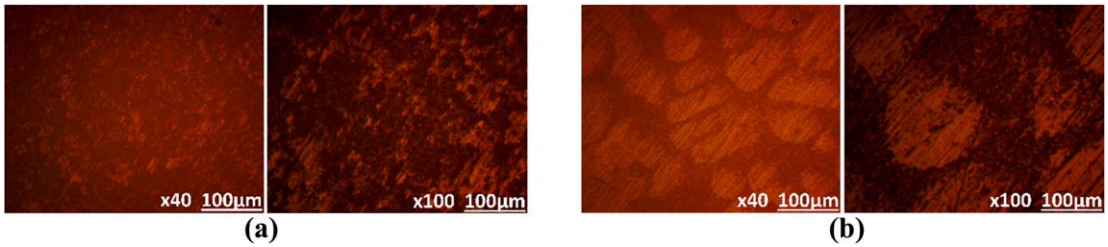

Figure 11. Microscopic images of (a) 3004Al and (b) 4044Al from 0.1 M H_2SO_4 solution.

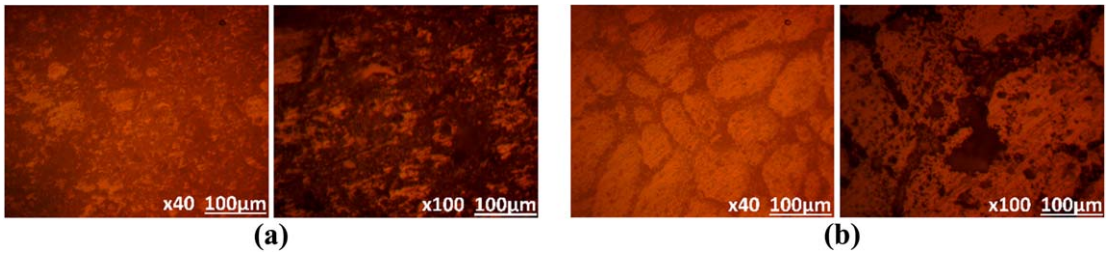

Figure 12. Microscopic images of (a) 3004Al and (b) 4044Al from 0.00625 M 0.1 M H_2SO_4 solution at 0.5% NaCl concentration.

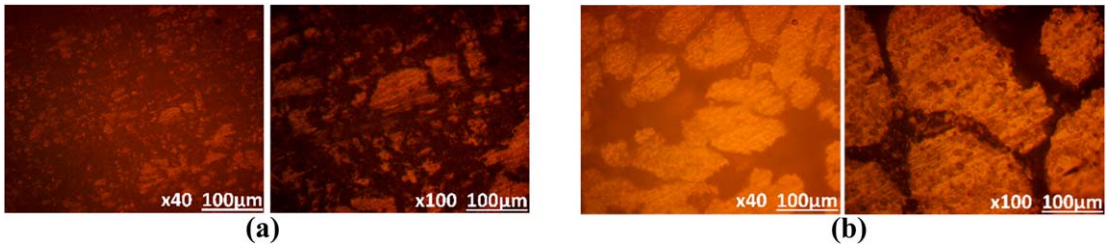

Figure 13. Microscopic images of (a) 3004Al and (b) 4044Al from 0.1 M H_2SO_4 solution at 0.5% NaCl concentration.

4044Al from 0.00625 M H_2SO_4 solution at 0.5% and 4.5% NaCl concentrations. The optical images in figures 7(a) and (b) depicts the surface of the alloys and significant variation in microstructural properties. Grain boundaries are clearly visible on 4044Al due to the presence of Si which contributes to the heterogeneity of its microstructural and metallurgical characteristics. This contrasts the marginally homogeneous morphology of 3004Al due to the high solubility of Mg alloying element and the limited solubility of Mn responsible for the formation of most of its intermetallic phases. The morphology of figures 8(a) to 9(a) significantly differs from the morphology in figures 8(b) to 9(b). General surface deterioration is visible in figures 8(a) to 9(a) due to the electrochemical action of Cl^- ions, though the marginal homogeneous microstructure of 3004Al is responsible for this. It must be noted that closer observation shows deterioration was also present at some grain boundaries. The nature of deterioration on figures 8(b) to 9(b) tends to be along the grain boundary. Limited deterioration

occurred on the substrate aluminium alloy. 3004Al and 4044Al morphologies agrees with the results from potentiodynamic polarization where 3004Al exhibited weaker resistance to general corrosion compared to 4044Al. However, potentiostaic studies showed 4044Al exhibited weak resistance to localized corrosion. Figures 10(a) to 11(a) shows the extent of 3004Al surface deterioration by SO_4^{2-} ions significantly differs from the action by Cl^- ions. While the deterioration by Cl− ions tends to be partially localized to a large extent, deterioration by SO_4^{2-} ions occurred throughout the entire surface. Whereas, the morphology of 4044Al in figures 10(b) to 11(b) depicts the appearance of more grain boundaries and deterioration along the boundaries. In the presence of combined chloride-sulphate the extent of deterioration on 3004Al [figures 12(a) and 13(a)] remained generally the same despite higher rate of corrosion from electrochemical test. However, observation of figures 12(b) and 13(b) shows the extent of deterioration along the grain boundaries is much higher and deeper due to extensive localized corrosion. Even the morphology outside the grain boundaries deteriorated compared to the separate electrochemical action of Cl^- and SO_4^{2-} ions.

4. Conclusion

4044Al underwent significant localized deterioration along its grain boundaries from optical microscopy observations due to its heterogeneous microstructure compared to 3004Al. Electrochemical analysis showed the formation of weak passive film on its surface which easily collapsed in the presence of chloride ions. However, in the presence of chloride and sulphate ions, the alloy exhibited significant resistance to general corrosion. 3004Al sustained its passive film at all chloride concentrations due to it continuous nature and solubility of its alloying elements. The alloy underwent stable pitting at generally the same potential. In contrast to the observation for 4044Al, the localized corrosion resistance of 3004Al is appreciable, though the alloy was displayed relatively weak resistance to general corrosion. Both alloys were generally thermodynamically stable in the electrolytes though potential transients were visible in the presence of chloride ions.

Data availability statement

All data that support the findings of this study are included within the article (and any supplementary files).

ORCID iDs

Roland T Loto https://orcid.org/0000-0002-1675-8989

References

[1] Birbilis N T, Muster T H and Buchheit R G 2011 Corrosion of aluminium alloys *Corrosion Mechanisms in Theory and Practice* 3rd edn (Boca Raton, FL: CRC Press) 705–36
[2] Zhang Z, Yang X, Zhang J, Zhou G, Xu X and Zou B 2011 Effect of welding parameters on microstructure and mechanical properties of friction stir spot welded 5052 aluminum alloy *Mater. Des.* **32** 4461–70
[3] The aluminium association (https://aluminum.org/aluminum-advantage/facts-glance)
[4] Alaneme K K, Olubambi P A, Afolabi A S and Bodurin M O 2014 Corrosion and tribological studies of bamboo leaf ash and alumina reinforced Al-Mg-Si alloy matrix hybrid composites in chloride medium *Int J Elect Sci* **9** 5663–74 http://www.electrochemsci.org/papers/vol9/91005663.pdf
[5] Asif M, Chandra K and Misra P S 2011 Development of aluminium based hybrid metal matrix composites for heavy duty applications *Journal of Minerals and Materials Characterization and Engineering* **10** 1337–44
[6] Prasad D S, Shoba C and Ramanaiah N 2014 Investigations on mechanical properties of aluminum hybrid composites *J Mater Res Technol* **3** 79–85
[7] Staley J T 2016 Corrosion of aluminium aerospace alloys *Mater. Sci. Forum* **877** 485–91
[8] Long R S, Boettcher E and Crawford D 2017 Current, and future uses of aluminium in the automotive industry *Journal of Minerals* **69** 2635–9
[9] Davis J R 1999 *Corrosion of Aluminum and Aluminum Alloys* (Materials Park, OH: ASM International) https://www.asminternational.org/documents/10192/1849770/06787G_Sample.pdf/c4151917-99fc-46e8-a310-d5578d0af160
[10] Loto R T and Babalola P 2018 Effect of alumina nano-particle size and weight content on the corrosion resistance of AA1070 aluminum in chloride/sulphate solution *Results Phys* **10** 731–7
[11] Loto R T 2019 Investigation of the influence of SiC content and particle size variation on the corrosion resistance of Al-SiC matrix composite in neutral chloride solution *Int J Adv Manuf Tech* **101** 2407–13
[12] Loto R T and Babalola P 2019 Corrosion resistance of low SiC particle variation at low weight content on 1060 aluminum matrix composite in sulfate-contaminated seawater *Results Phys* **13** 102241
[13] Nam N D, Phung V D, Thuy P T P, Dao V A, Kim S H and Yi J S 2019 Corrosion behaviours of hot-extruded Al-xMg alloys *J Mater Res Techn* **8** 5246–53
[14] Rana R S, Purohit R and Das S 2012 Reviews on the influences of alloying elements on the microstructure and mechanical properties of aluminum alloys and aluminum alloy composites *International Journal of Scientific and Research Publications* **2** 1–7 http://www.ijsrp.org/research_paper_jun2012/ijsrp-June-2012-10.pdf

[15] Hurlen T, Lian H, Odegard O S and Valand T V 1984 Corrosion and passive behaviour of aluminium in weakly acid solution *Electrochim. Acta* **29** 579–85
[16] Mountarlier V, Gigandet M P, Normand B and Pagetti J 2005 EIS characterisation of anodic films formed on 2024 aluminium alloy, in sulphuric acid containing molybdate or permanganate species *Corros. Sci.* **47** 937–51
[17] Lukovits I, Kalman E and Zucchi F 2001 Corrosion inhibitors—Correlation between electronic structure and efficiency *Corrosion* **57** 3–9
[18] Brett C M A, Gomes I A R and Martins J P S 1994 The electrochemical behaviour and corrosion of aluminium in chloride media. The effect of inhibitor anions *Corros. Sci.* **36** 915–23
[19] Solange P-D, Benjamín H P, Rosario Á G and Mauro B V 2011 Study of pitting corrosion of the commercial aluminium alloy AA3003 in saline environment *Rev Tec Fac Ing Univ* **34** 108–23 http://ve.scielo.org/scielo.php?pid=S0254-07702007000400020&script=sci_abstract&tlng=en
[20] Natishana P M and O'Grady W E 2014 Chloride ion interactions with oxide-covered aluminum leading to pitting corrosion: a review *J. Electrochem. Soc.* **161** C421–32
[21] Szklarska-Smialowska Z 1999 Pitting corrosion of aluminium *Corros. Sci.* **41** 1743–67
[22] Zaid B, Saidi D, Benzaid A and Hadji S 2008 Effects of pH and chloride concentration on pitting corrosion of AA6061 aluminum alloy *Corros. Sci.* **50** 1841–7
[23] Šeruga M and Hasenay D 1996 Corrosion of aluminium in soft drinks *Z Lebensm Unters Forch* **202** 308–12
[24] Husaini M, Usman B and Ibrahim M B 2018 Evaluation of corrosion behaviour of aluminum in different environment *Bayero Journal of Pure and Applied Sciences* **11** 88–92 https://www.ajol.info/index.php/bajopas/article/view/182839
[25] Bolzoni F, Contreras G, Lazzari L, Ormellese M, Pérez E, Re G and Benedetti A 2011 Influence of chloride and sulphate content on the performance of aluminium based galvanic anodes *Corros. Rev.* **29** 287–96
[26] Oya Y, Honkawa Y and Kojima Y 2014 Pitting corrosion of aluminum alloy in chloride solution cantaining sulfate and sulfite ion *Zairyo-to-Kankyo* **63** 394–400
[27] Hou X, Gao L, Cui Z and Yin J 2018 Corrosion and protection of metal in the seawater desalination *IOP Conf. Ser.: Earth Environ. Sci.* **108** 022037
[28] Hajar H M, Zulkifli F, Mohd Sabri M G and Wan Nik W B 2016 Protection against corrosion of aluminum alloy in marine environment by lawsonia inermis *Int J Corros* 4891803
[29] Nnaji N, Nwaji N, Mack J and Nyokong T 2019 Corrosion resistance of aluminum against acid activation: impact of benzothiazole-substituted gallium phthalocyanine *Molecules MDPI* **24** 207
[30] Xhanari K, Finšgar M, Hrnči M K, Maver U, Knez Z and Seiti B 2017 Green corrosion inhibitors for aluminium and its alloys: a review *RSC Adv.* **7** 27299–330
[31] Klodian X and Matjaž F 2019 The corrosion inhibition of AA6082 aluminium alloy by certain azoles in chloride solution: electrochemistry and surface analysis *Coatings* **9** 380
[32] Abd-El-Naby B A, Abdullatef O A and El-Mahmody W A 2017 Effect of surfactants on the corrosion behavior of aluminum in acid solutions containing chloride ions *Physical Chemistry* **7** 1–7
[33] Lorking K F and Mayne J E O 1966 The corrosion of aluminium in solutions of sodium fluoride and sodium chloride *Br. Corros. J.* **5** 181–2
[34] Foly R T 1975 Complex ions and corrosion *J. Electrochem. Soc.* **122** 1493
[35] Bhattamishra A K and Banerjee M K 1993 Corrosion behaviour of Al-Zn-Ms alloys in nacl solution in presence of cerium salts *Int. J. Mater. Res.* **84** 734–6
[36] Koroleva E V, Thompson G E, Hollrigl G and Bloeck M 1999 Surface morphological changes of aluminium alloys in alkaline solution: effect of second phase material *Corros. Sci.* **41** 1475–95
[37] Moon S M and Pyun S I 1997 The corrosion of pure aluminium during cathodic polarization in aqueous solutions *Corros. Sci.* **39** 399–408
[38] Vargel C 2004 The influence of oxygen dissolved in water *Corrosion of Aluminium* (Amsterdam: Elsevier) (https://doi.org/10.1016/B978-0-08-044495-6.X5000-9)
[39] Aziz I, Qi Z and Min X 2009 Corrosion inhibition of SiCp/5A06 aluminum metal matrix composite by cerium conversion treatment *Chinese J Aeronaut* **22** 670–6
[40] Reboul M and Meyer P 1987 Intergranular and exfoliation corrosion study of Al-LiCu-Mg-Zr alloys *J. Phys.* **48** 881–9
[41] Trowsdale A J, Noble B, Harris S J, Gibbins I S R, Thompson G E and Wood G C 1996 The influence of silicon carbide reinforcement on the pitting behaviour of aluminium *Corros. Sci.* **38** 177–91
[42] Huang Y 2018 *Materials Corrosion and Protection, 3. Electrochemical Corrosion Kinetics* (Berlin: De Gruyter) (https://doi.org/10.1515/9783110310054-003)
[43] Holzer F, Muller S, Desilvestro J and Haas O 1993 Aluminium alloys in sulphuric acid: I. Electrochemical behaviour of rotating and stationary disc electrodes *J. Appl. Electrochem.* **23** 125–34
[44] Drazic D M, Zecevic S K, Atanasoki R T and Despic A R 1983 The effect of anions on the electrochemical behaviour of aluminium *Electrochim. Acta* **28** 751–5
[45] Bennour I, Maurice V and Marcus P 2010 X-ray photoelectron spectroscopy study of the interaction of ultra-thin alumina films on NiAl alloys with NaCl solutions *Surf. Interface Anal.* **42** 581–7
[46] Martin F J, Cheek G T, Grady W E O and Natishan P M 2005 Impedance studies of the passive film on aluminium *Corros. Sci.* **47** 3187–201
[47] Esquivel J and Gupta R K 2020 Review—corrosion-resistant metastable al alloys: an overview of corrosion mechanisms *J. Electrochem. Soc.* **167** 081504
[48] Ralston K D, Fabijanic D and Birbilis N 2011 Effect of grain size on corrosion of high purity aluminium *Electrochim. Acta* **56** 1729
[49] Serna L M, Zavadil K R, Johnson C M, Wall F D and Barbour J C 2006 A critical implanted cl concentration for pit initiation on aluminum thin films *J. Electrochem. Soc.* **153** B289
[50] Chen K, Liu C, Yang J, Ma P, Zhan L and Huang M 2020 Stabilizing Al–Mg–Si–Cu alloy by precipitation nano-phase control *Mater. Sci. Eng. A* **769** 138513
[51] Wang J, Zhang B, Zhou Y T and Ma X 2015 Multiple twins of a decagonal approximant embedded in S-Al2CuMg phase resulting in pitting initiation of a 2024Al alloy *Acta Mater.* **82** 22–31
[52] Wang J, Zhang B, Wu B and Ma X L 2016 Size-dependent role of S phase in pitting initiation of 2024Al alloy *Corros. Sci.* **102** 183–9
[53] Starke E A and Staley J T 1996 Application of modern aluminum alloys to aircraft *Prog. Aerosp. Sci.* **32** 131–72

[54] Donatus U, Thompson G E, Omotoyinbo J A, Alaneme K K, Aribo S and Agbabiaka O G 2017 Corrosion pathways in aluminium alloys *Trans. Nonferrous Met. Soc. China* **27** 55–62
[55] Stannard T J, Williams J J, Singh S S, Sundaram Singaravelu A S, Xiao X and Chawla N 2018 3D time-resolved observations of corrosion and corrosion-fatigue crack initiation and growth in peak-aged Al 7075 using synchrotron X-ray tomography *Corros. Sci.* **138** 340–52
[56] Ralston K D, Birbilis N, Cavanaugh M K, Weyland M, Muddle B C and Marceau R K W 2010 Role of nanostructure in pitting of Al–Cu–Mg alloys *Electrochim. Acta* **55** 7834–42
[57] Ameer M A, Fekry A M and El-Taib Heakal F 2004 Electrochemical behaviour of passive films on molybdenum-containing austenitic stainless steels in aqueous solutions *Electrochim. Acta* **50** 43–9
[58] Boucherit N, Hugot-le Goff A and Joiret S 1992 Influence of Ni, Mo, and Cr on pitting corrosion of steels studied by Raman spectroscopy *Corrosion* **48** 569–79
[59] Tobler W J and Virtanen S 2006 Effect of Mo species on metastable pitting of Fe18Cr alloys—A current transient analysis *Corros. Sci.* **48** 1585–607
[60] Bastidas J M, Torres C L, Cano E and Polo J L 2002 Influence of molybdenum on passivation of polarised stainless steels in chloride environment *Corros. Sci.* **44** 625–33
[61] Zamin M 1981 The role of Mn in the corrosion behavior of Al-Mn alloys *Corrosion* **37** 627–32
[62] Nam S W and Lee D H 2000 The effect of Mn on the mechanical behavior of Al alloys *Met. Mater.* **6**
[63] Vargel C 2020 chapter B.5 - Influence of alloy composition *Corrosion of Aluminium* 2ed edn127–55
[64] Tait W S 2018 Electrochemical corrosion basics *Handbook of Environ. Degrad. Mater.* Third Ed. (Amsterdam: Elsevier Inc) 97–115
[65] Esmailzadeh S, Aliofkhazraei M and Sarlak H 2018 Interpretation of cyclic potentiodynamic polarization test results for study of corrosion behavior of metals: A Review *Prot Met Phys Chem Surfaces* **54** 976–89
[66] Halambek J, Cindrić I and Ninčević Grassino A 2020 Evaluation of pectin isolated from tomato peel waste as natural tin corrosion inhibitor in sodium chloride/acetic acid solution *Carbohydr Polym* **234** 115940
[67] Seri O 1994 The effect of NaCl concentration on the corrosion behavior of aluminum containing iron *Corros. Sci.* **36** 1789–803
[68] Asduzzaman M D, Mustafa C M and Mayeedul I 2011 Effects of concentration of sodium chloride solution on the pitting corrosion behavior of AISI-304L austenitic stainless steel *Chem Ind Chem Eng Q* **17** 477–83
[69] Moravcik I, Peighambardoust N S, Motallebzadeh A, Moravcikova-Gouvea L, Liu C, Prabhakar J M, Dlouhy I and Li Z 2021 Interstitial nitrogen enhances corrosion resistance of an equiatomic CoCrNi medium-entropy alloy in sulfuric acid solution *Mater. Charact.* **172** 110869